Chapter

Design and CFD Analysis on the Reduction of Thermal Effect in Re-entry Vehicle by Using Retractable Aerospike

Pradeep Kumar Sulur Loganathan

Abstract

The shape optimization of two spike classes was investigated in this study. A spike with a sharp and blunt spikes reduces drag and aero-thermodynamic heating and enables longer ranges for economical flight. Conversion of kinetic energy into heat when coming down to earth causes damage—the blunt nose design increases maximum temperature and density at the vehicle's nose. Sharp-fore bodies reduce drag but provide only an area for dispersing heat flux downstream of the shock wave—the increased area of a blunt fore-body aids in efficient heat dissipation. ANSYS Fluent is used to analyze blunt bodies with blunt and sharp spike configurations, as well as the effect of counter flow. The findings suggest drag reductions ranging from 44% to 61%. The twin-spike design is the best among the models studied, with a 44 percent reduction in peak heat flux and a 46 percent reduction in the drag coefficient. Thermal protection systems, commonly used to reduce heat in re-entry vehicles, are costly. The aim of this study is to minimize re-entry heating by introducing a spike in the frontal region of the nose and preventing further vehicle damage at high temperatures.

Keywords: aero thermodynamic heating, ablating materials, blunt and sharp spikes

1. Introduction

The sporadic creation of the shock layer is one of the features of hypersonic flow. The shock wave is attached to the completely tangent to the nose cone and is known as an attached shock wave when the structural bluntness ratio is equal to zero. The shock separation distance grows when the boundary layer rises more significantly than zero. The shock wave will intensify, and the shock layer will grow thicker. In the shock layer, the BR factor raises static pressure, temperature, and density while lowering velocity [1]. Aero heating in hypersonic flow is also affected by the large-scale separated vortex generated by the shock wave and boundary layer interaction near the head cone. The vortex has a strong pulsation pattern and produces heat skin

depressions due to structural deformation in a thicker boundary layer and a fluctuating temperature distribution. The formation and dissolution of the vortex cause violent vibration [2].

Variations in the thermodynamic nonequilibrium conditions are caused by the dissociation patterns produced by the multiple gas mixtures. The shock wave is located further away from the vehicle surface because it is upstream of the vehicle surface in the airflow. It has been discovered that approximately 30% of the original air composition is dissociated, whereas the percentage in CO_2 flow is around 60%; as a result, energy transfer in the translational-rotational modes in airflow is slower than in CO_2 [3]. An Orion-like re-entry capsule's multidisciplinary design optimization (MDO) produced more effective design solutions than the low-fidelity aero thermodynamic model. Future developments may consider chemical nonequilibrium phenomena to refine aero thermodynamic implications and heat load estimation considerations [4].

The cohesive zone method (CZM) was used to determine the region for delamination propagation in a re-entry vehicle's ceramic matrix composites body flap. Due to the low longitudinal strength under compression and compressive load, no growth is possible for the maximum allowed delamination size as an existing manufacturing defect (5 mm) and under the maximum hinge moment service condition. The development of extensive delamination increased due to the impact of foreign objects. The margin of safety concerning the investigated body flap's delamination growth phenomenon is nearly 20 in the most critical service load conditions [5].

Because compressible flows are hyperbolic, the leading bow shock influences the wake region. The increased energy available for chemical reactions, which leads to the formation of new atomic compositions, is accompanied by an increase in number density over the bow shock. The bow shock temperature decreases for all energy states, and the highest temperature values are found within the shock layer, indicating that chemical reactions can change the thickness of the shockwave structures and the distribution of thermodynamic properties across the domain [6].

To improve oxidation resistance while maintaining thermomechanical stability, adhesion, and homogeneity, a commercial product made of Al-oxide-based refractory varnish was enhanced with silicon-oxide nanoparticles. The carbon-carbon-coated materials resist erosion and oxidation and have excellent morphology with no visible discontinuities [7]. Thermal coating, also known as the thermal protection system (TPS), is required for re-entry vehicles. Thermal barrier coating (TBC) is used to resist large temperature gradients because metals are highly susceptible to corrosion, heating, and wear. We use phenolic and composites, such as silica and ceramics. This module will discuss the challenges encountered during re-entry, desirable vehicle shapes, materials used to prevent aerodynamic heating, types of re-entry vehicles, and brief analysis of their performance [8].

Because of atmospheric drag and aerodynamic heat, the planet's gravity and atmosphere place enormous strain on spaceflight during entry. This project concerns the CFD analysis in ANSYS Fluent of the entry capsule with a payload into the Earth's atmosphere. The shockwave behavior during the module's entry will be investigated [9]. The mechanical properties of silica aerogels with various geometric properties, such as particle size, pore size, and ligament diameter, were calculated using the finite volume method (FVM). According to the FVM simulation results, a power law

correlation exists between relative density and mechanical properties (elastic modulus and yield stress) of silica aerogels. Finally, the findings suggest that it is possible to create silica aerogels with an ultra-low density, high strength, and stiffness if the textural features are well controlled [10].

The evaluation of the re-entry vehicle's aero thermodynamic analysis. The flow field around a blunted cone-flare in hypersonic flow is depicted using computational fluid dynamics results. The heat flux was calculated using a numerical approach to the Navier-Stokes equation and two different Mach numbers [11]. This study studies the effect of thermal loads on the structure and observes how it reacts because of the thermal loads, providing exposure to various coupled-field analyses [12].

The study's goal was to perform a thermostructural analysis of the TPS of a re-entry module known as the Crew module. The thermostructural research includes heat transfer analysis to determine temperature distribution and variation throughout the operation. The thermal and mechanical load analysis is then performed to obtain structural deformations and stresses [13]. This article discusses the nose cone, the forwardmost section of a rocket, guided missile, or aircraft. The cone is shaped to provide the least amount of aerodynamic resistance. Nose cones are also intended for use in and under water and on high-speed land. The nose cone of a satellite vehicle may become the satellite itself after separating from the rocket's final stage, or it may be used to shield the satellite until the orbital speed is achieved before separating from the satellite [14, 15].

2. Introduction- Aero thermodynamic heating

Atmospheric entry is the movement of an object from outer space into and through the gases of a planet's, dwarf planets, or natural satellite's atmosphere. Uncontrolled entry, such as the entry of astronomical objects, space debris, or bolides, and controlled entry (or) re-entry of a spacecraft capable of being navigated or following a predetermined course are the two main types of atmospheric entry. EDL refers to the technologies and procedures that allow for the controlled atmospheric entry, descent, and landing of spacecraft. Atmospheric and aerodynamic heating can cause atmospheric breakup capable of completely disintegrating smaller objects. These forces may cause things with lower compressive strength to explode. Before parachutes or air brakes can be deployed, crewed space vehicles must be slowed to subsonic speeds. Such vehicles have kinetic energies ranging from 50 to 1,800 megajoules, and atmospheric dissipation is the only way to expend the kinetic energy. The rocket fuel required to slow the vehicle would be nearly equal to the amount used to accelerate it initially, making the use of retro rockets for the entire Earth re-entry procedure impractical [8].

While adiabatic compression causes the high temperature at the heat shield's surface, the vehicle's kinetic energy is eventually lost due to gas friction (viscosity) after the vehicle has passed by. Other minor energy losses include direct black body radiation from hot gases and chemical reactions between ionized gases [14]. Ballistic warheads and expendable vehicles do not require slowing during re-entry and are designed to maintain speed. Furthermore, slow-speed returns to Earth from near-space, such as parachute jumps from balloons, do not necessitate heat shielding because the gravitational acceleration of an object starting at relative rest within the

atmosphere (or not far above it) cannot generate enough velocity to cause significant atmospheric heating [16].

At the Karman line, 100 km (62.14 mi/54 nautical mi) above the surface, atmospheric entry occurs for Earth. In comparison, Venus atmospheric entry occurs at 250 km (155.3 mi/135 nautical mi), and Mars atmospheric entry occurs at about 80 km (50 mi/43.2 nautical mi). Uncontrolled objects accelerate through space toward the Earth under gravity and are slowed by friction when they come into contact with the Earth's atmosphere. Meteors are often relatively fast relative to the Earth because their orbital path differs from the Earth's before encountering the Earth's gravity [17]. Most controlled objects enter at hypersonic, orbital, or unbounded speeds. Several technologies have been developed to enable atmospheric re-entry and flight at high speeds. Buoyancy is a low-velocity controlled atmospheric entry method suitable for planetary entry where thick atmospheres, strong gravity, or both complicate high-velocity hyperbolic entry, such as the atmospheres of Venus, Titan, and the gas giants [1].

2.1 Thermal effects on space re-entry vehicle

The primary cause of shock-layer heating is not direct friction with the re-entry object. Some heating is also accounted for by friction-based entropy increases of the molecules within the wave [2]. It has little effect when the vehicle travels at subsonic speeds. Still, it significantly impacts the design, material of the vehicle structure, and the incorporated systems at supersonic (beyond M = 1.2) and hypersonic (beyond M = 5) speeds. The spacecraft re-enters at very high speeds (Mach number greater than 20), which is enough to destroy the vehicle if safety precautions are not taken. Even after the vehicle has reached a high stability temperature, the heating effect remains at its high point at the leading edge [3].

2.2 Aerospike

During the flight, hypersonic vehicles experience significant drag and aerodynamic heating. Many attempts are being made to reduce these impacts to achieve longer ranges, reduced fuel consumption, and safer flights. One method is to employ spikes. A spike is a needle-like body attached to the main Blunt's nose tip [16]. The primary mechanism of drag and heating reduction is twofold: first, a much weaker oblique foreshock replaces the strong detached bow shock ahead of the blunt body; second, it encourages separation of the flow downstream of the foreshock and creates a recirculation zone that screens a large portion of the main body nose surface. The shear layer that encircles the recirculation zone reattaches to the main body surface, creating a shock wave that turns the outer flow at the body shoulder [17].

Several designs are being considered. Spikes, aero discs, and even supersonic projectiles that were thrown ahead of the blunt forebody are among the concepts. Among these strategies, spikes proved to be the most straightforward and successful in minimizing aerodynamic heating [2]. A drag-reducing aerospike minimizes the aerodynamic drag of blunt bodies at supersonic speeds. A detached shock is created ahead of the body by the aerospike. A zone of recirculating flow forms between the shock and the forebody, acting as a more streamlined forebody profile and lowering drag [10].

3. Silica aerogel

3.1 Silica aerogel: A historical overview

Many people believe that aerogels are recent technological advancements. The first aerogels were made in 1931. Steven. S. Kistler of the College of the Pacific in Stockton, California, set out at the time to prove that a "gel" contained a continuous solid network the same size and shape as the wet gel. The obvious way to test this hypothesis was to remove the liquid from the wet gel without causing any damage to the solid component. As is often the case, the apparent path was fraught with peril. When a wet gel is left to dry on its own, it shrinks, often to a fraction of its original size. This shrinkage was frequently accompanied by severe gel cracking. Kistler correctly predicted that the solid component of the gel was microporous and that the evaporating liquid's liquid-vapor interface exerted strong surface tension forces that collapsed the pore structure. Kistler then discovered the most crucial aspect of aerogel [13].

The first gels studied by Kistler were silica gels prepared by the acidic condensation of aqueous sodium silicate. However, attempts to prepare aerogels by converting the water in these gels to a supercritical fluid failed. Instead of leaving a silica aerogel behind, the supercritical water redissolved the silica, precipitating as the water was vented. When the French government approached Stanislaus Teichner at Claud Bernard University, Lyon, in the late 1970s, he was looking for a method to store oxygen and rocket fuels in porous materials. What happened next is the subject of a legend passed down among aerogel researchers. Teichner delegated the task of preparing and studying aerogels for this application to one of his graduate students [18].

Particle physics researchers realized in the early 1980s that silica aerogels would be an ideal medium for producing and detecting Cherenkov radiation. Large transparent tiles of silica aerogel were required for these experiments. Two large detectors were built using the TMOS method. One at the Deutsches Elektronen-Synchrotron (DESY) in Hamburg, Germany, used 1700 L of silica aerogel in the TASSO detector, and another at CERN used 1000 L of silica aerogel prepared at the University of Lund in Sweden [19]. The Lund group established the first pilot plant in Sjobo, Sweden, to produce silica aerogel monoliths using the TMOS method. A 3000-L autoclave was included in the plant to handle the high temperatures and pressures encountered in supercritical methanol production (240°C and 80 atmospheres). However, during a production run in 1984, the autoclave developed a leak. The room in which the vessel was kept quickly filled with methanol vapors and exploded. The plant was later rebuilt and still produces silica aerogels through the TMOS process [20].

3.2 Energy absorbing materials

Simply said, materials absorb kinetic energy by plastic deformation, elastic deformation, brittle fracture, or the fluid dynamics of gases or liquids inside the material. Organic foams, such as expanded polystyrene, polyurethanes, polyethers, or polyethylene, are frequently employed as impact-absorbing materials. These often exhibit plastic or elastomeric behavior [9]. As an inorganic solid, silica aerogels are fragile by nature. At first, glance, using delicate material as cushioning could appear bad. Because silica aerogels typically contain shallow-density elements, the solid

network collapses gradually, distributing the force of impact over a more extended period. Additionally, because silica aerogels are an open-pored substance, the gas inside the solid's central portion is driven outside when the material collapses [15].

3.3 Environmental concerns

Silica aerogels are produced and used in an environmentally friendly manner. During their manufacture, no significantly dangerous wastes are produced. Silica aerogels can be disposed of naturally. They swiftly break down into a fine powder in the environment that resembles one of the most prevalent materials on Earth, sand, almost precisely. Silica aerogels are also absolutely nontoxic and inflammable. They could eliminate a tremendous quantity of unnecessary plastic materials if they ever make their way into general use as protective materials [21].

3.4 Potential uses

Silica aerogels may find utility in various applications due to their appealing energy-absorbing qualities. These could include safeguarding one's safety while driving, safeguarding delicate equipment such as aircraft flight recorders, and safeguarding technological devices such as laptop hard drives [22].

3.5 The pore structure of silica aerogel

Silica aerogels' pore structure is challenging to define in words. Unfortunately, the approaches for describing porosity that is now available only somewhat improve on that. According to a categorization proposed by the International Union of Pure and Applied Chemistry, pores with a diameter of less than 2 nm are called "micropores," those between 2 and 50 nm are called "mesopores," and those more than 50 nm are called "macropores." [23].

4. Thermal properties of silica aerogels

Around 1980, there was a resurgence of interest in aerogel technology as energy efficiency, and the environmental implications of chlorofluorocarbons (CFCs) became more of a concern. The solid insulating value and environmentally benign manufacturing processes of silica aerogels made them an appealing replacement for conventional insulation, which became immediately apparent. Unfortunately, cost-sensitive businesses like housing could not afford the material's production costs [24]. There are three processes by which thermal energy can travel through an insulating material: solid conductivity, gaseous conductivity, and radiative (infrared) transmission. These three factors add up to the material's overall thermal conductivity. A given material's inherent quality is solid conductivity. Solid conductivity is comparatively high for dense silica. However, only a tiny (1–10%) portion of solid silica is present in silica aerogels. As a result, thermal transfer through the silica aerogel's substantial component takes a very circuitous route and is not incredibly efficient. The visual transparency of silica aerogels makes them ideal for insulation applications. The radioactive component of thermal transfer is small and unimportant at low temperatures [25].

4.1 Thermal resistance

The aerogel particles on the fabric surface increase the fabric's thermal resistance. The thermal resistance of the thickener-coated material was 0.0118 m^2K/W, whereas the thermal resistance of the aerogel-coated fabric (A1) was 0.0199 m^2K/W. In other words, a 2% aerogel coating increased thermal resistance by 68.64%.

5. Synthesis of the aerogels

Melamine (M), Resorcinol (R), and Formaldehyde (F) were polycondensed to form hydrogels with sodium carbonate as a catalyst (C) and deionized water (W) as a solvent. Carbon black (CB) and diatomite were used as conductive and anti-shrinkage additives. The reactants used in the gel preparation had molar ratios of (M + R)/C of 135 and (M + R)/W of 0.052. By adding acetic acid or sodium carbonate, the final pH of the precursors was eventually adjusted to pH 7.4. The samples for the MRF series were created using a pre-polymerization procedure described elsewhere. For 1 hour at 40°C, a solution containing R, F, C, and (solution A) was stirred. Separately, at 70°C, a solution containing M, F, W, and C (solution B) was stirred for 30 minutes. Then, solutions A and B were mixed and stirred for 20 minutes at room temperature to allow the precursors to cross-link further [26].

Diatomite (50% w/v) and carbon black (ca.0.9wt %) were added before gelification, and k was required to ensure a homogeneous dispersion. Following the gelatine step, the hydrogels were supercritically dried with CO_2 after a controlled water-acetone exchange. Finally, the carbon aerogels were carbonized in a nitrogen atmosphere to produce denser carbon aerogels [20].

6. Heat ablating materials

6.1 Phenolics-impregnated carbon ablators (PICA)

Phenolics-impregnated carbon ablators (PICA), a carbon fiber preform impregnated in phenolics resin, is a modern thermal production system with the advantages of low density coupled with efficient ablative ability at high heat flux. It is a good choice for ablative applications such as high peak heating conditions found on the sample or lunar return missions. Phenolics-impregnated carbon ablators' thermal conductivity is lower than other heat flux ablative materials, such as conventional carbon phenolics [27].

PICA was the primary TPS material for the Stardust Aeroshell and was patented by NASA Ames Research Centre in the 1990s. The sample-return capsule Stardust was the fastest artificial object to re-enter Earth's atmosphere (12.4 km/s (28,000 mph) at 135 km altitude), 70% faster than the Shuttle and the Apollo mission capsules. PICA was critical to the success of the Stardust mission, which returned to Earth in 2006. The heat shield on Stardust (0.81 m base diameter) was made of one monolithic piece that could withstand a nominal peak heating rate of 1.2 kW/cm^2. A PICA heat shield was also used for the Mars Science

Laboratory's entry into the Martian atmosphere. During atmospheric entry, the resin and carbon fibers decay at different rates, resulting in distinct zones in the material.

- The virgin material, which has not decomposed.
- The char layer has entirely decomposed the resin. As the carbon fibers decompose, the heat shield contracts.
- The pyrolysis zone is formed by interpolating between the virgin and char layers.
- PICA-NuSil, also known as PICA-N, is a type of PICA. The addition of NuSil reduces the spread of phenolic dust found in PICA and improves the heat shield's integrity by making it more resistant to humidity and erosion [28].

PICA is a simple ablative TPS composed of a porous chopped carbon fiber preform infused with a high-surface area phenolic resin matrix. Because the phenolic infusion is at a low loading level, the final material is highly porous and has a low density. As a result, the ablative material is relatively efficient. The risk of massive cost or long endurance redevelopment for PICA required to support the next decade's priority planetary entry missions is currently rated low to moderate [29].

6.2 Ultra-high-temperature ceramic (UHTC) materials

Ultra-high-temperature ceramic (UHTC) materials are a class of refractory ceramics that offer excellent stability at temperatures above 2000°C. They are being researched as potential thermal production system (TPS) coatings for material subjected to high temperatures and bulk material for heating elements. Borides, carbides, nitrides, and oxides of early transition metals are examples of ultra-high-temperature ceramics [30]. The current effects have concentrated on heavy, early transition metal borides like hafnium diboride (HfB_2) and zirconium diboride (ZrB_2). Hafnium nitride (HfN), zirconium nitride (ZrN), titanium carbide (TiC), titanium nitride (TiN), titanium dioxide (ThO_2), tantalum carbide (TaC), and their associated composites are other ultra-high-temperature ceramic materials under investigation for thermal production system (TPS) applications.

Due to the completion of Space Shuttle missions and the elimination of Air Force space plane development. However, a series of NASA programs in the 1990s aimed at developing a fully reusable hypersonic space plane, such as the National Aerospace Plane, Venture star/X-33, Boeing X-37, and the Air Force's Black star program, UHTCs were also increasingly used in a variety of settings, ranging from nuclear engineering to aluminum production [11]. NASA Ames conducted two flight experiments in 1997 and 2000 to test the real-world performance of UHTC materials in re-entry environments. By mounting them on modified nuclear ordnance Mk12A re-entry vehicles and launching them on Minuteman III ICBMs, the slender Hypersonic Aerothermodynamic Research Probes (SHARP B1 and B2) briefly exposed the UHTC materials to actual re-entry environments.

SHARP-B2 was recovered and included four retractable, sharp wedge-like protrusions called "strakes" that each contained three different UHTC compositions extended into the re-entry flow at different altitudes to improve the characterization of UHTC mechanical strength and better study their performance [15]. The SHARP-B2 test allowed the recovery of four segmented strakes, each with three sections made of a different HfB_2 or ZrB_2 composite. Despite impacting the sea at three times the predicted velocity, the vehicle was successfully recovered. Between 14 and 19 seconds into re-entry, four rear strake segments (HfB_2) fractured, two mid components (ZrB_2/SiC) cracked, and no fore strake segments failed [4].

The actual heat flux was 60% lower than predicted, the actual temperatures were much lower, and the heat flux on the rear strakes was much higher than expected. Material failures in composites and pure ceramics were caused by enormous grain sizes, with cracks following macroscopic crystal grain boundaries [16]. Because of their high melting points and good mechanical properties, UHTCs will become vital components as the next generation of spacecraft, and hypersonic flight applications are developed [12]. Only small, simple-shaped bulk UHTC components can be formed due to the limitations of current processing methods. UHTC coatings can be used to solve this problem. As C- and SiC-based composites become more widely used as structural components in aeronautics, protective coatings will be required to protect them from the harshest environments [31].

6.3 Toughened uni-piece fibrous reinforced oxidation composites (TUFROCs)

The toughened uni-piece fibrous reinforced oxidation composite (TUFROC) allows space launch facilities and other frameworks that use earth re-entry vehicles to be much more affordable and sustainable. The TUFROC's exposed surface design and the appropriate material combination will allow a space vehicle to withstand both the mechanical stresses of initial ascent and the extreme heating and stress of re-entry. It provides a thermal production tile attachment system suitable for application to the leading edge of a space vehicle and other uses in extreme heating environments up to 36000°F, possibly higher for short intervals [3].

The variant of TUFROC tested and reported here was 0.4 g/cm^3. It was created to operate at surface temperatures of around 2000 K. In conjunction with the ROCCI 4 cap, the graded surface treatment provides dimensional stability during high-speed entries. In contrast, the fibrous base insulation offers low thermal conductivity insulation to protect the vehicle structure [7]. The advantage of this low-cost, insulating composite over a re-entry vehicle with a sharp leading edge is increased cross-range capability due to reduced drag. The reinforced carbon-carbon (RCC) has large radii and operates at heat fluxes of less than 70 W/cm^2 during Earth entry. These systems are significantly heavier than TUFROC (1.6 g/cm^3 vs. 0.4 g/cm^3), orders of magnitude more expensive, and require substantially longer fabrication lead times (**Figures 1–19**) [5].

When a lightweight fibrous TPS, such as TUFI-treated AETB, is applied to a vehicle's wing leading edge, it is susceptible to excessive recession during re-entry. Because of the temperature capability of the two-piece TUFROC TPS technology, lightweight fibrous insulation can be applied to a space vehicle's wing leading edge (**Table 1**) [32].

7. 3D view of space re-entry vehicle

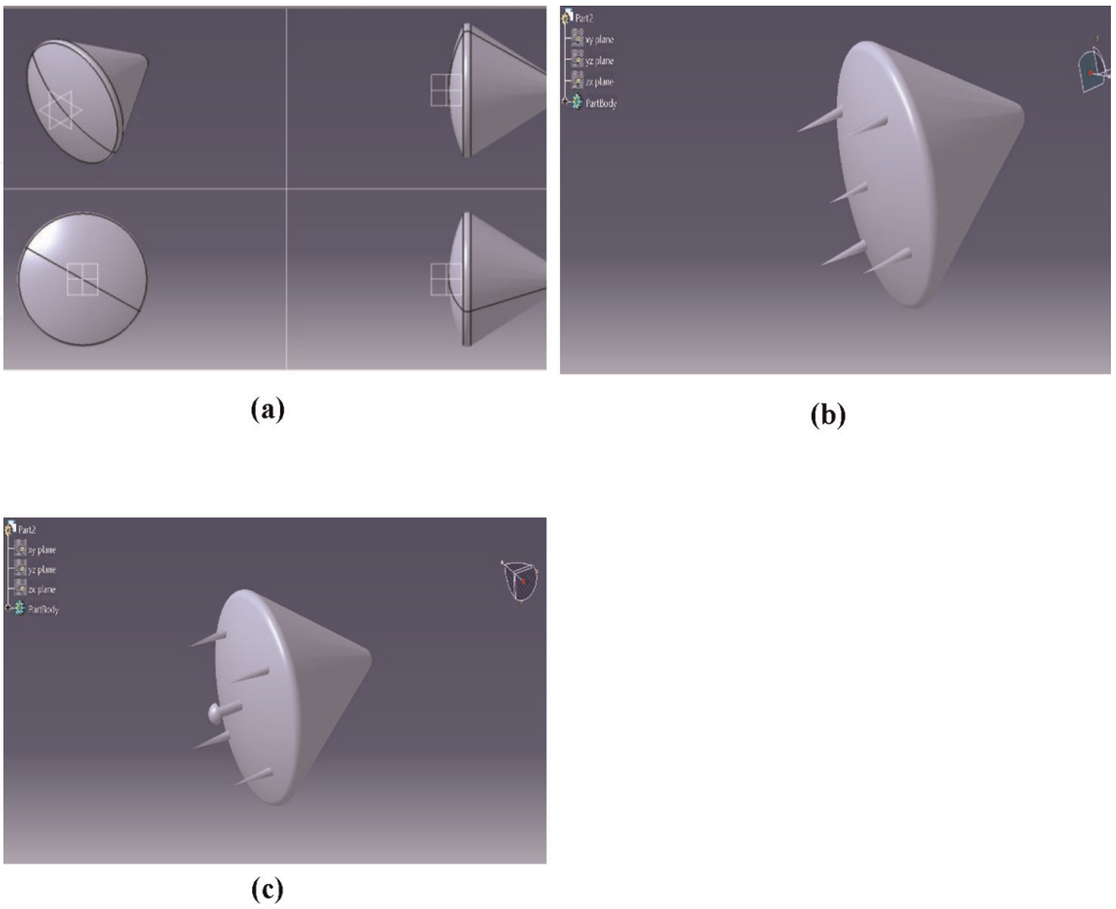

Figure 1.
a. 3D view of space re-entry vehicle, b. with sharp spike, c. with blunt spike.

8. Result and discussion

8.1 PICA

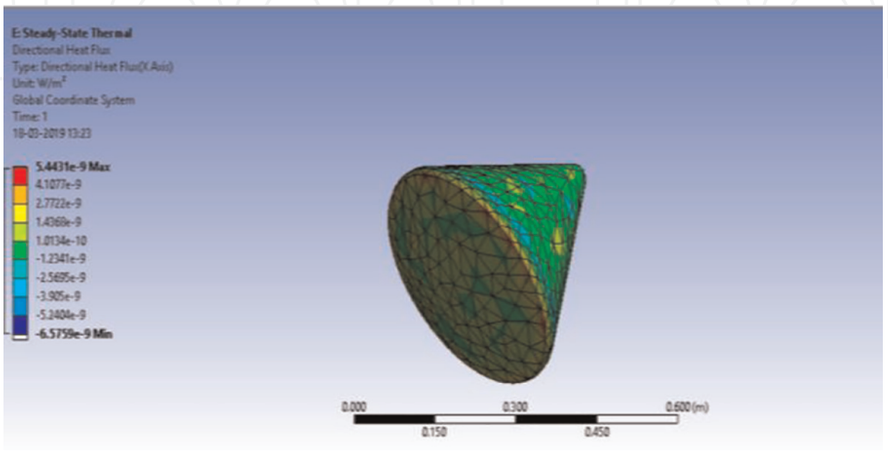

Figure 2.
Directional heat flux steady state in PICA.

DOI: http://dx.doi.org/10.5772/intechopen.107841

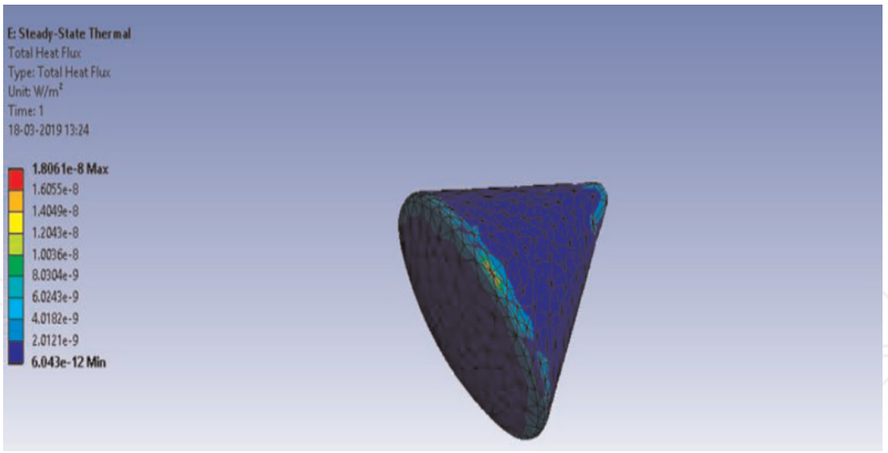

Figure 3.
Total heat flux steady state in PICA.

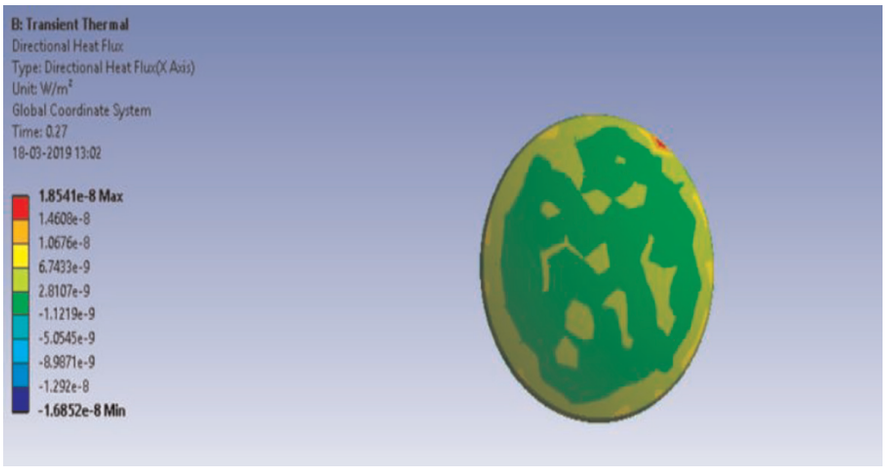

Figure 4.
Directional heat flux transient in PICA.

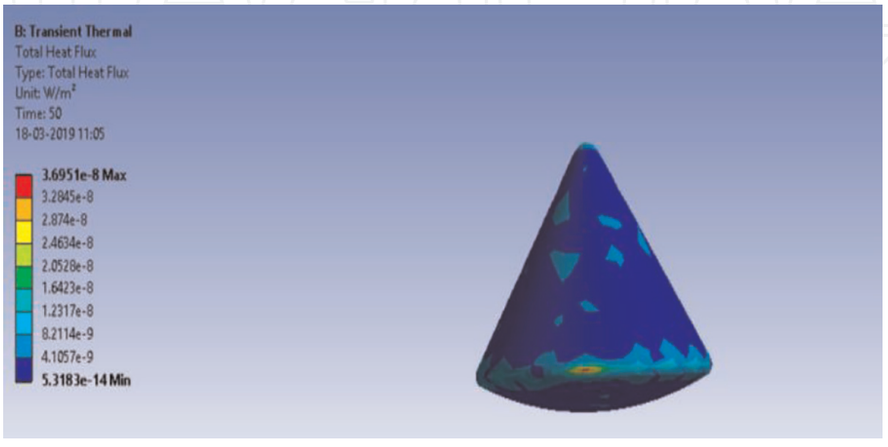

Figure 5.
Total heat flux transient in PICA.

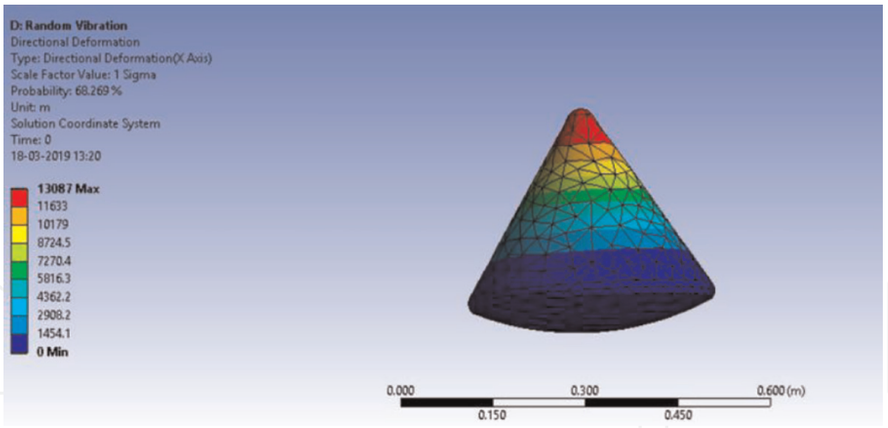

Figure 6.
Directional deformation—vibration in PICA.

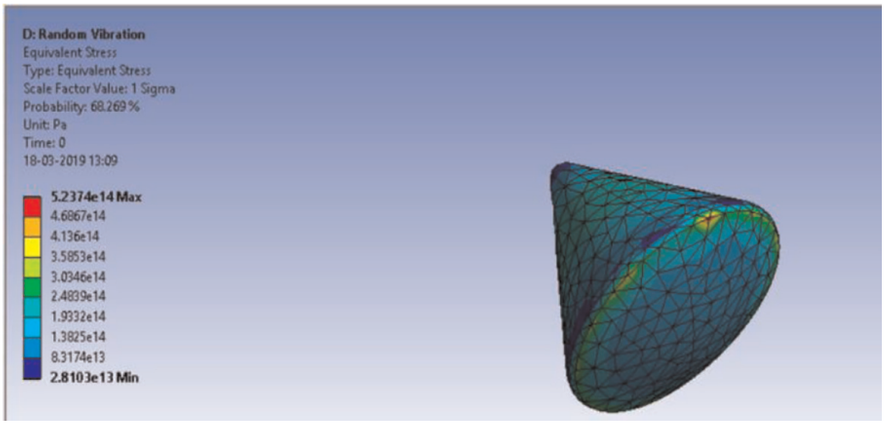

Figure 7.
Equivalent stress—vibration in PICA.

8.2 TUFROC

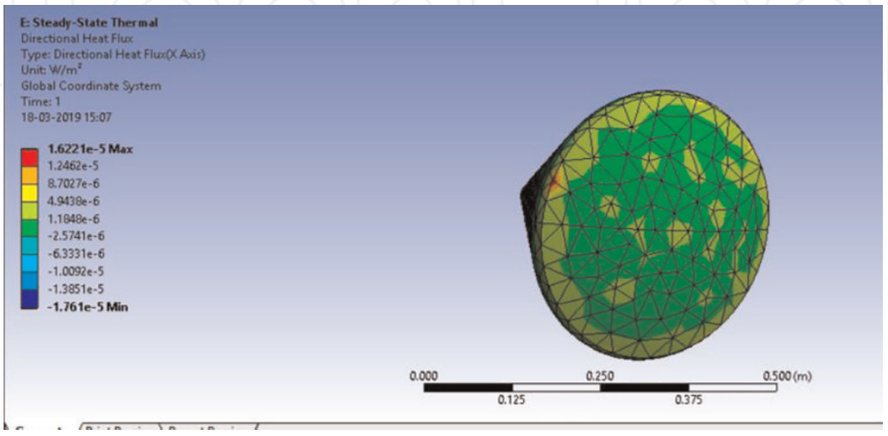

Figure 8.
Directional heat flux steady state in TUFROC.

DOI: http://dx.doi.org/10.5772/intechopen.107841

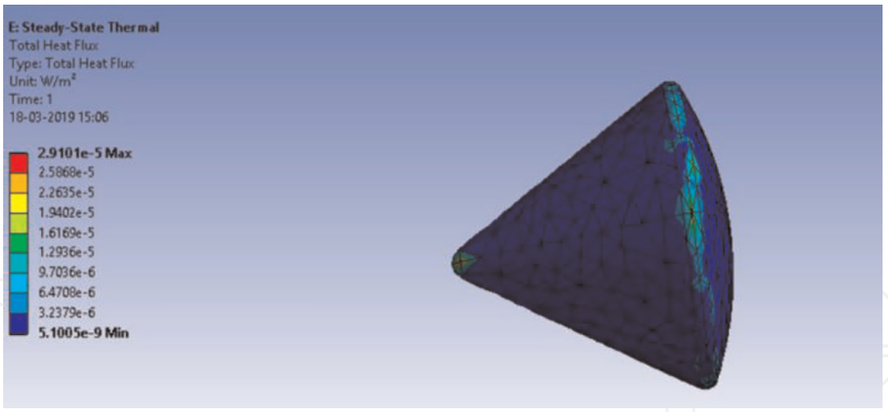

Figure 9.
Total heat flux steady state in TUFROC.

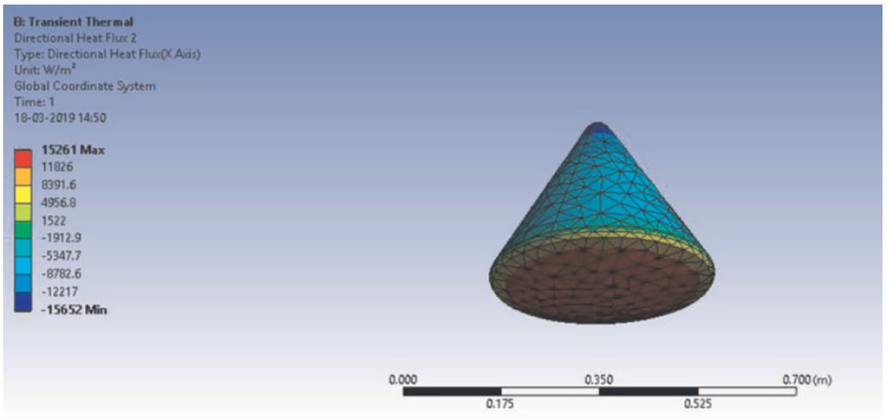

Figure 10.
Directional heat flux transient in TUFROC.

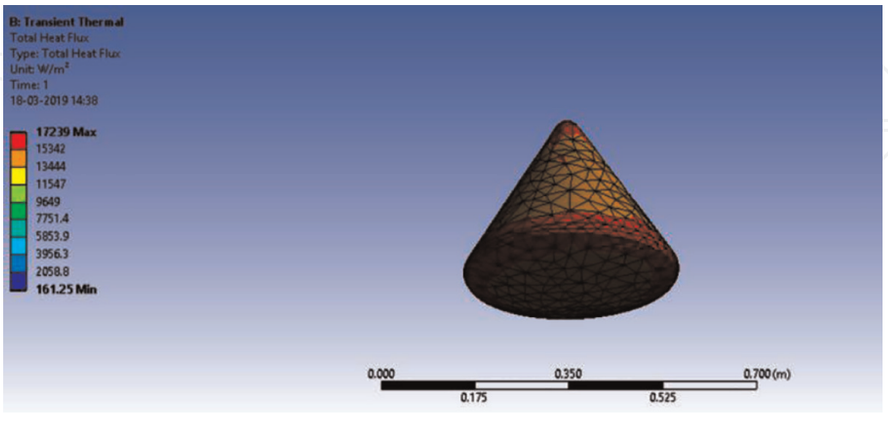

Figure 11.
Total heat flux transient in TUFROC.

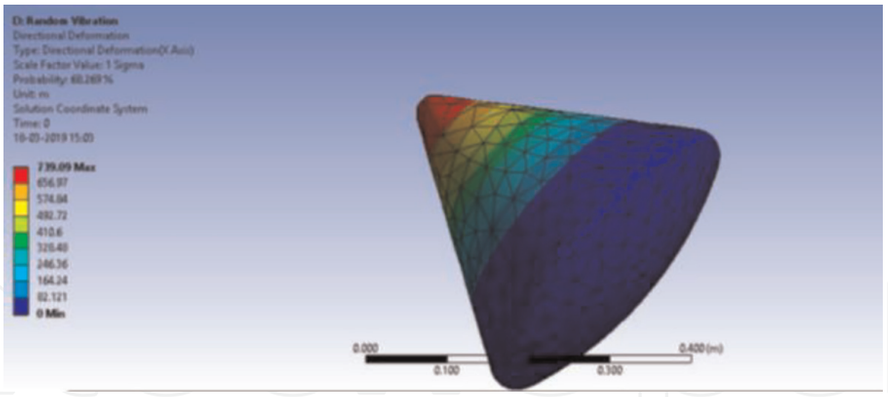

Figure 12.
Directional deformation—vibration in TUFROC.

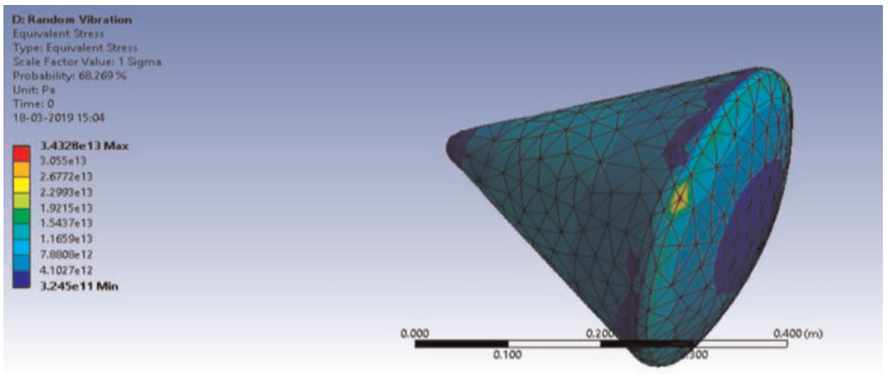

Figure 13.
Equivalent stress—vibration in TUFROC.

8.3 UHTC

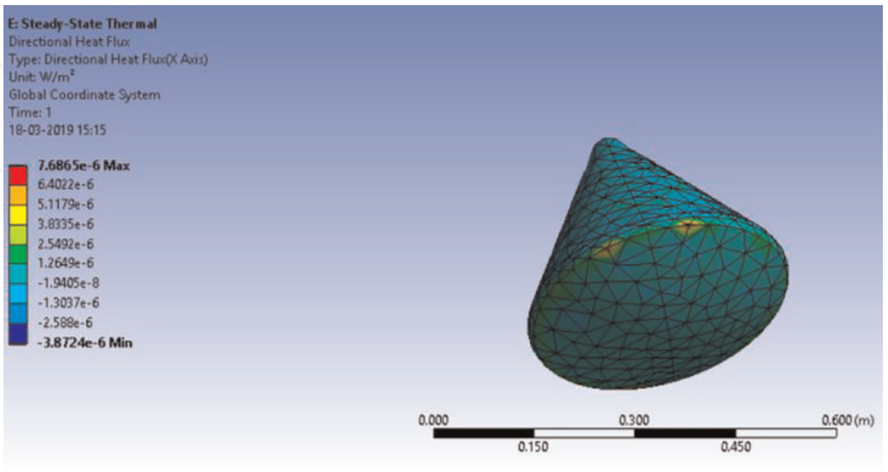

Figure 14.
Directional heat flux steady state in UHTC.

DOI: http://dx.doi.org/10.5772/intechopen.107841

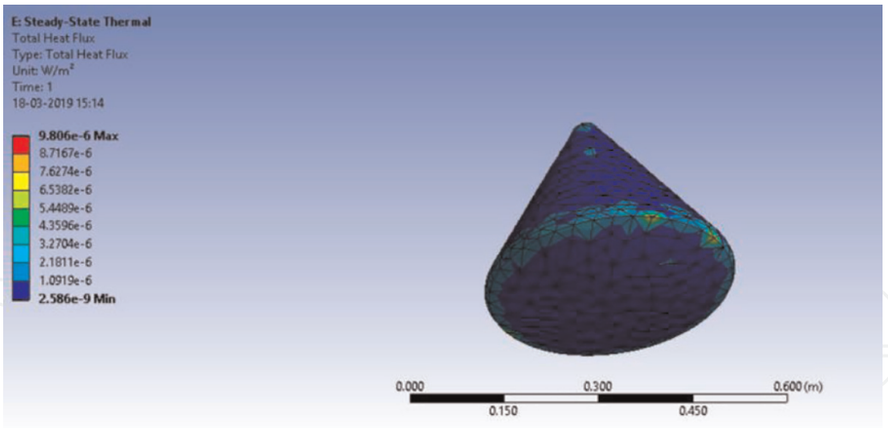

Figure 15.
Total heat flux steady state in UHTC.

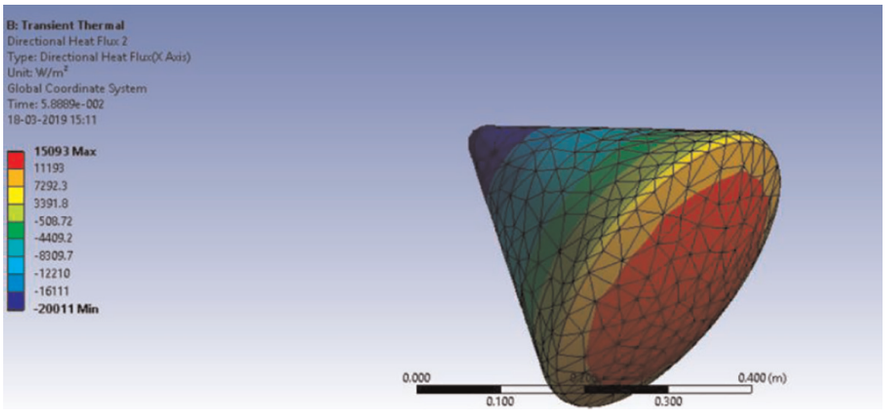

Figure 16.
Directional heat flux transient in UHTC.

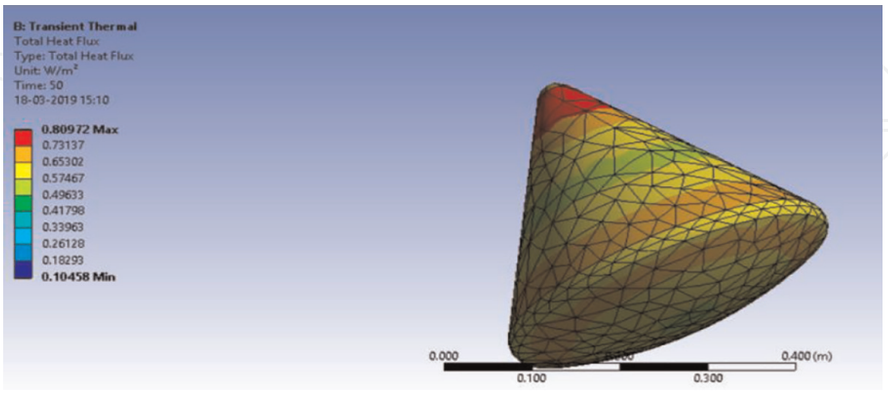

Figure 17.
Total heat flux transient in UHTC.

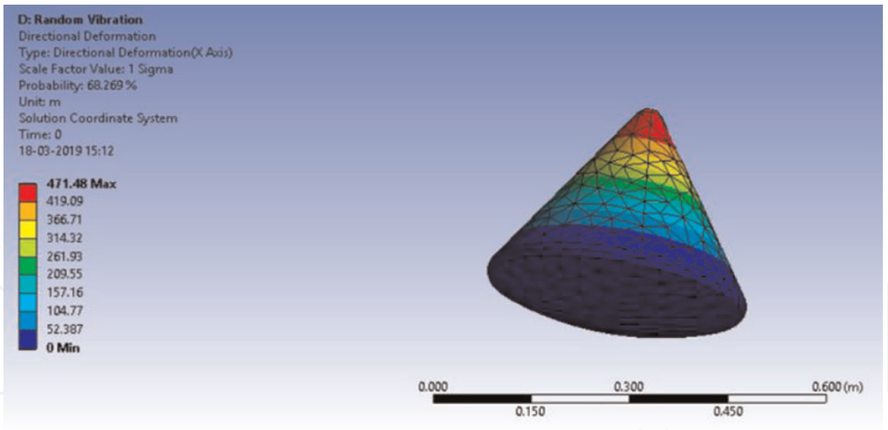

Figure 18.
Directional deformation—vibration in UHTC.

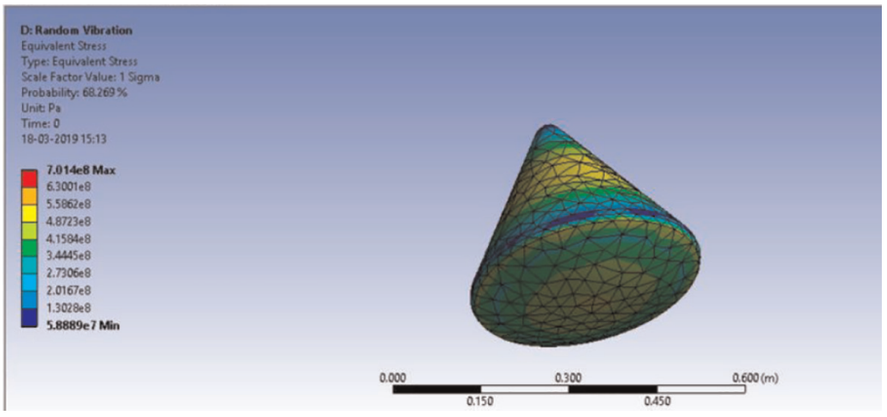

Figure 19.
Equivalent stress—vibration in UHTC.

Properties	Ultra-high-temperature ceramic (UHTC) material	Toughened uni-piece fibrous reinforced oxidation composites (TUFROCs)	Silica aerogel
Poisson ratio	0.12–0.14	0.5	0.2
Young's modulus	360 G pa	70 (or) 7 GPa	10^6–10^7 N/m^2
Density	6.10 g/cm^3	0.27 g/cm	0.003–0.35 g/cm^3
Temperature	Above 2000°C	3600°F(1982.22°C)	Above 1200°C
Thermal conductivity	75–105 w/mk	219–221 w/mk	0.5 W/mk
Isotropic resistivity	22 μ Ω cm	12–14 Ωcm	1e^{o23}*10^{-8} Ωm
Tensile ultimate strength	565 M Pa	4400 Mpa	45 to 155 Mpa
Compressive ultimate strength	6.14–12.5 M Pa	20.7Mpa	1100–1600 Mpa
Specific heat	56–83.8 Wm	1125 J/kg-k	330 K

Table 1.
Mechanical properties of different materials.

8.4 Silica aerogel

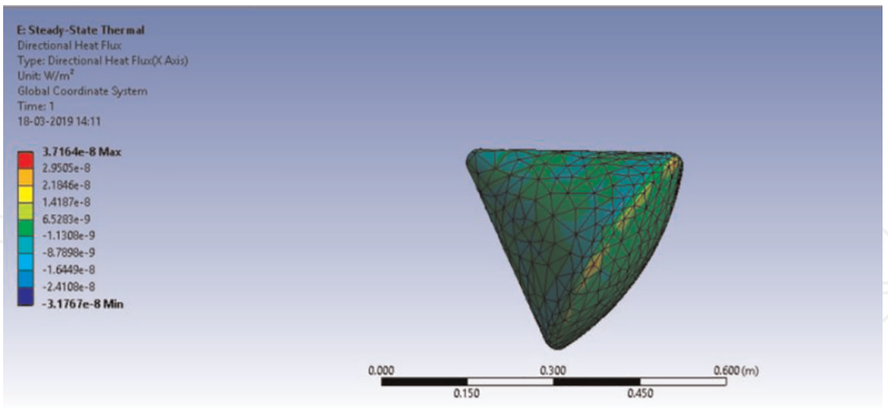

Figure 20.
Directional heat flux steady state in silica aerogel.

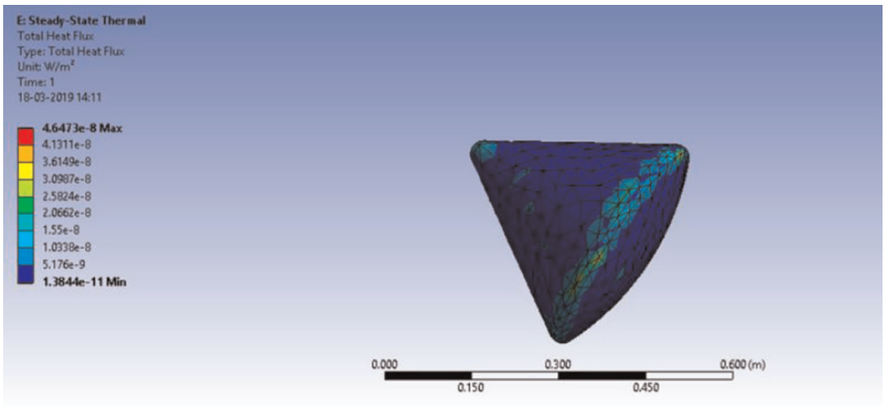

Figure 21.
Total heat flux steady state in silica aerogel.

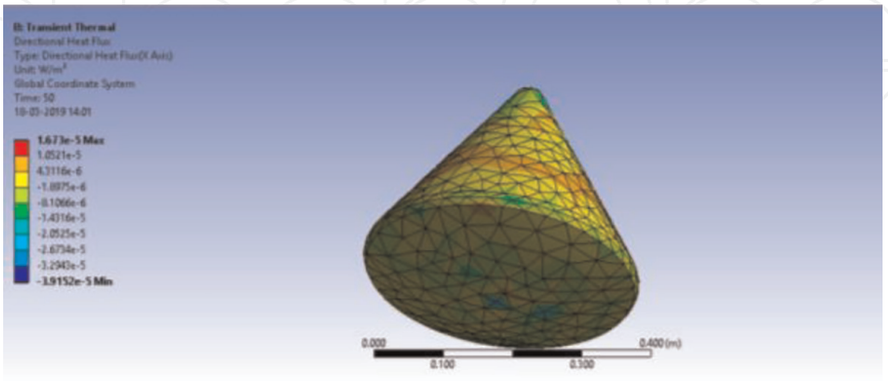

Figure 22.
Directional heat flux transient in silica aerogel.

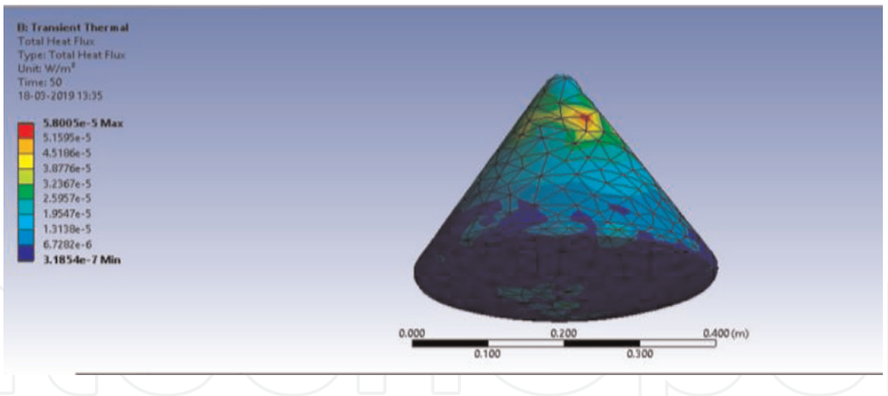

Figure 23.
Total heat flux transient in silica aerogel.

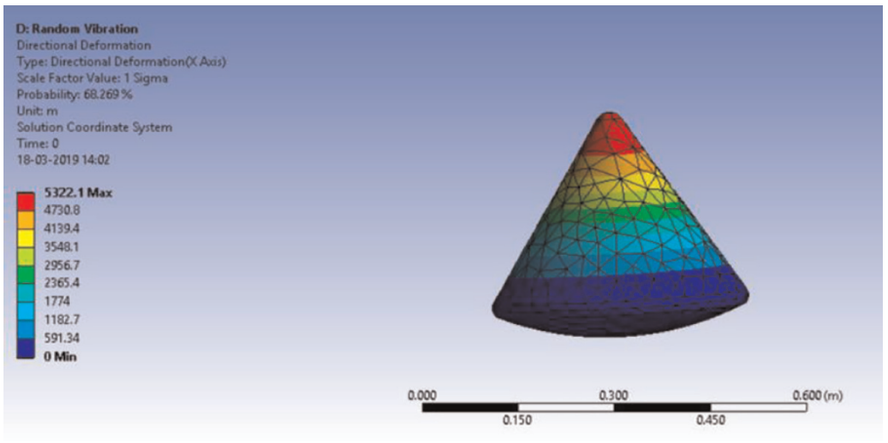

Figure 24.
Directional deformation—vibration in silica aerogel.

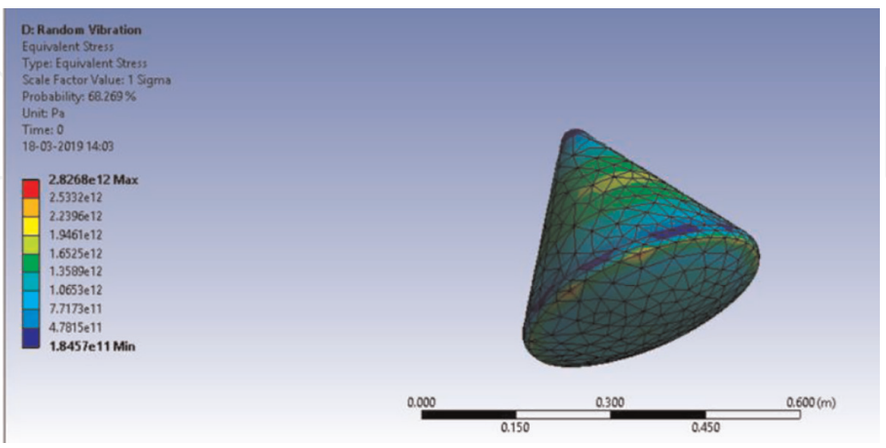

Figure 25.
Equivalent stress—vibration in silica aerogel.

9. Resultant table

The 3D modeling of the re-entry vehicle, with sharp and sharp-blend, is designed in CATIA which is shown in **Figure 1a**, **b**, and **c**. We have done the steady-state thermal analysis, transient thermal analysis, and vibration analysis on the space re-entry vehicle to analyze their thermal and vibration properties. In the first case, we discussed the steady-state thermal analysis for PICA in **Figures 2** and **3**, for TUFROC in **Figures 8** and **9**, for UHTC in **Figures 14** and **15**, and for silica aerogel in **Figures 20** and **21**; from this analysis, the silica aerogel has a low heat transfer value of $4.6473e^{-8}$ W/m^2 followed by PICA $5.8061e^{-8}$ W/m^2 from **Table 2**, which shows these materials will withstand the high temperature compared to the other materials. The silica aerogel is lightweight and has a high temperature-resisting property next to UHTC and TUFROC. In the second case, we discussed the transient thermal analysis for PICA in **Figures 4** and **5**, for TUFROC in **Figures 10** and **11**, for UHTC in **Figures 16** and **17**, and for silica aerogel in **Figures 22** and **23**; this analysis also shows that silica aerogel has a low heat transfer value of $5.8005e^{-5}$ W/m^2 from **Table 3**, followed by PICA $3.6951e^{-4}$ W/m^2, and the UHTC have 0.80972 W/m^2.

In the third case, we discussed the vibration analysis for PICA in **Figures 6** and **7**, for TUFROC in **Figures 12** and **13**, for UHTC in **Figures 18** and **19**, and for silica aerogel in **Figures 24** and **25**; from this analysis, the silica aerogel material has a high deformation sustaining the ability of 5322.1 W/m^2 due to the vibration effects on space re-entry vehicles compared to PICA 1308 W/m^2 from **Table 4**. This analysis shows that the silica aerogel can protect the parent material from the vibrations that occur during the re-entry into the atmosphere.

S. No	Directional heat flux steady state		Total heat flux steady state	
	Maximum (W/m^2)	Minimum (W/m^2)	Maximum (W/m^2)	Minimum (W/m^2)
UHTC	$7.6865e^{-6}$	$-3.8724e^{-6}$	$9.806e^{-6}$	$2.586e^{-9}$
PICA	$5.4431e^{-9}$	$-6.5759e^{-9}$	$5.8061e^{-8}$	$6.043e^{-12}$
TUFROC	$1.6221e^{-5}$	$-1.761e^{-5}$	$2.9101e^{-5}$	$5.1005e^{-9}$
SILICA AEROGEL	$3.7164e^{-8}$	$-3.1767e^{-8}$	$4.6473e^{-8}$	$1.3844e^{-11}$

Table 2.
Heat flux steady-state thermal analysis.

S. No	Directional heat flux transient		Total heat flux transient	
	Maximum (W/m^2)	Minimum (W/m^2)	Maximum (W/m^2)	Minimum (W/m^2)
UHTC	15093	−20011	0.80972	0.10458
PICA	$1.8541e^{-4}$	−1.685e-4	$3.6951e^{-4}$	$5.3183e^{-14}$
TUFRO	15261	−15652	17239	161.25
SILICA AEROGEL	1.673e–^{5}	$-3.9132e^{-9}$	$5.8005e^{-5}$	$3.1854e^{-7}$

Table 3.
Transient thermal analysis.

S. No	Directional deformation vibration		Equivalent stress vibration	
	Maximum (W/m^2)	Minimum (W/m^2)	Maximum (W/m^2)	Minimum (W/m^2)
UHTC	471.48	52.387	$7.014e^{8}$	$5.8889e^{7}$
PICA	1308	1454.1	$5.237e^{14}$	$2.8103e^{13}$
TUFROC	739.09	82.121	$3.4328e^{13}$	$3.245e^{11}$
Silica aerogel	5322.1	591.34	$2.8268e^{12}$	$1.8457e^{11}$

Table 4.
Random vibration analysis.

10. CFD Analysis

10.1 Pressure contours

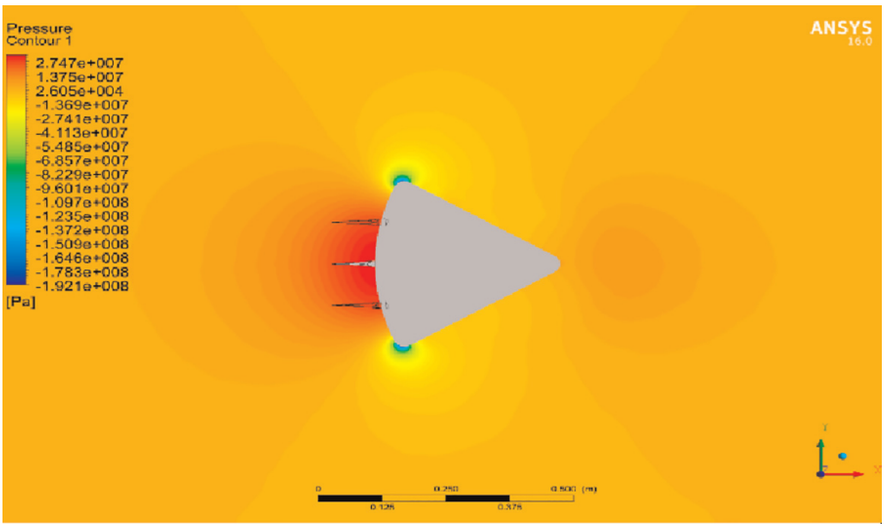

Figure 26.
Sharp spike.

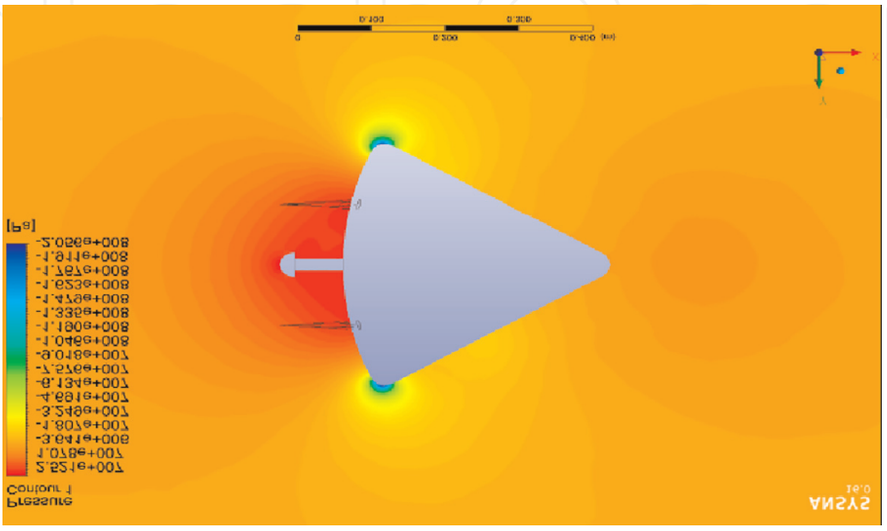

Figure 27.
Sharp with blunt spike.

DOI: http://dx.doi.org/10.5772/intechopen.107841

10.2 Velocity contours

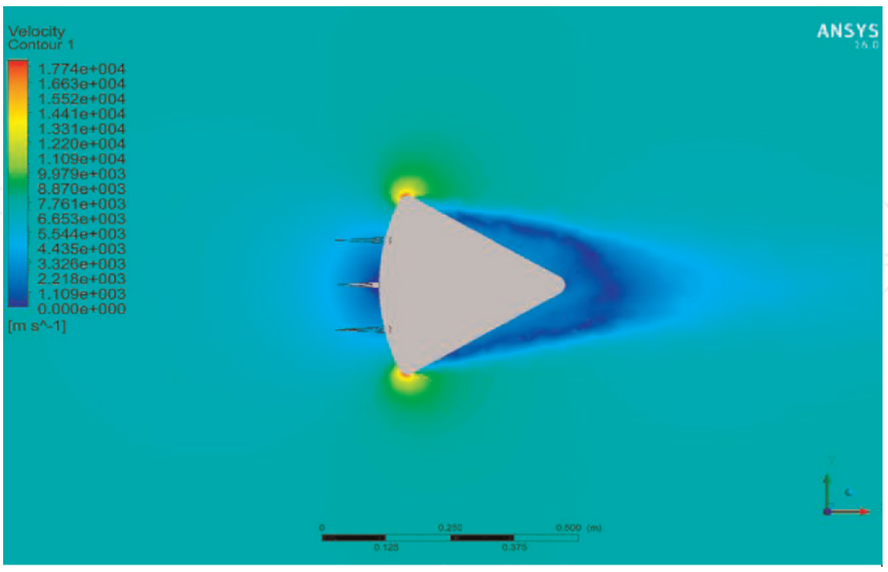

Figure 28.
Sharp spike.

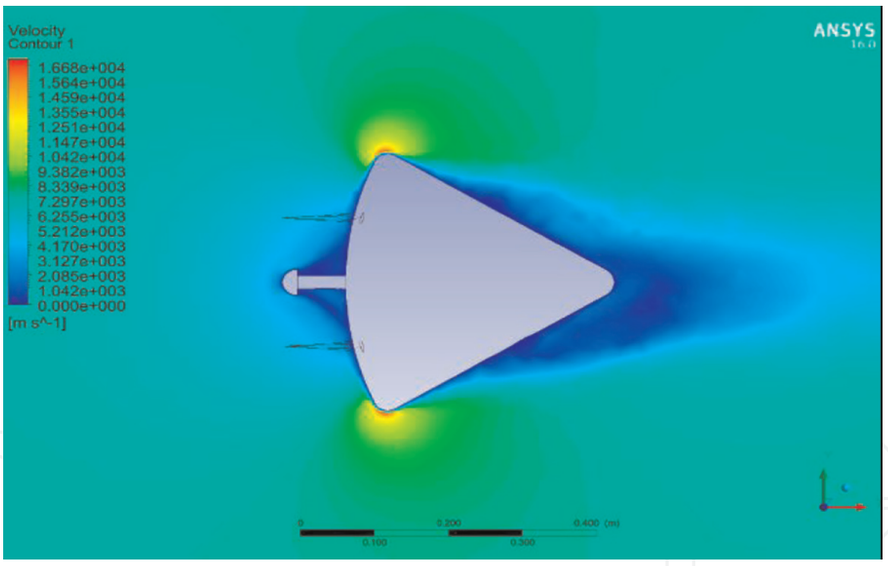

Figure 29.
Sharp with blunt spike.

10.3 Streamline flow

The flow analysis has done for re-entry vehicles with sharp spike and sharp-blunt spike combinations to examine the pressure shown in **Figures 26** and **27**, velocity shown in **Figures 28** and **29**, and streamline patterns shown in **Figures 30** and **31**. This analysis finds drag coefficient and shockwave formations in these two combinations. The analysis shows that these two combination re-entry vehicles with the aero disk with sharp aerospike have a drag value of 38641.5 N and

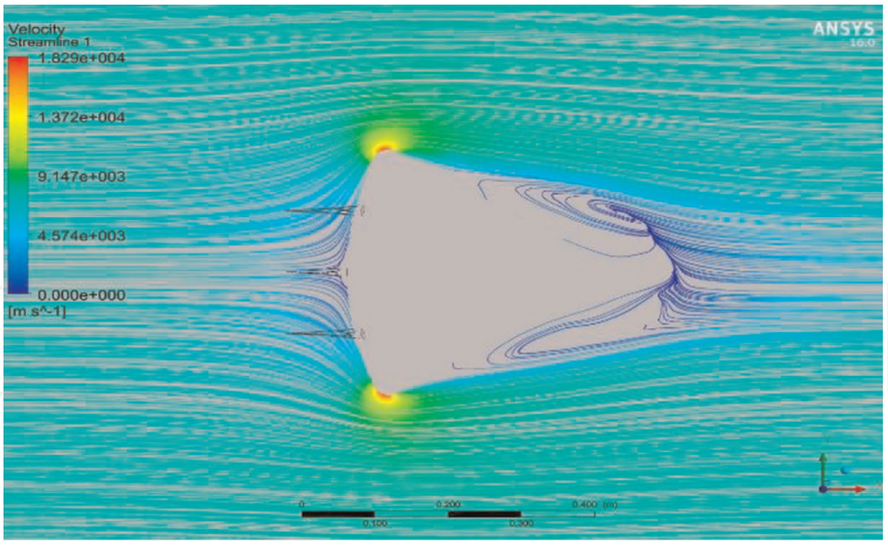

Figure 30.
Sharp spike.

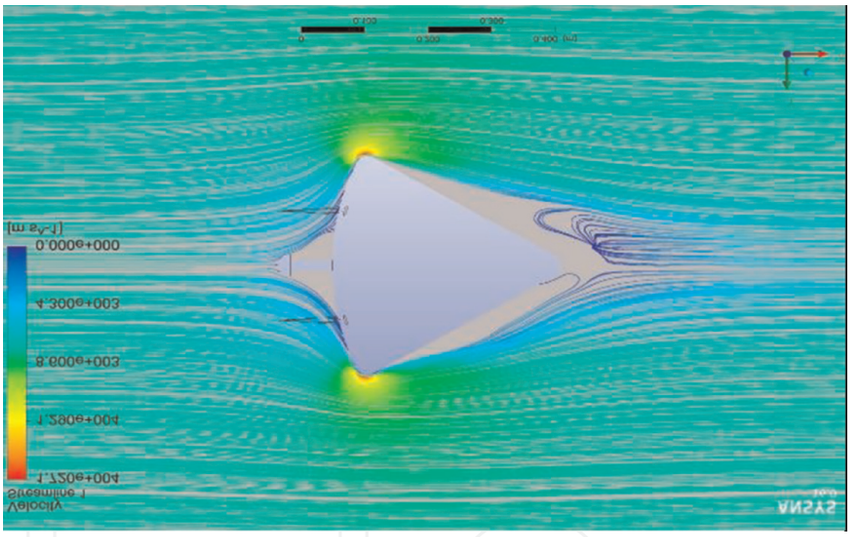

Figure 31.
Sharp with blunt spike.

lift the value of 11288.4 N, significantly reducing drag formation and the formation of shock waves. Whereas the spike with sharp-blunt has a drag value of 225718 N and lifts the value of 104559 N, this reduces the drag but is lesser than the previous sharp spike.

11. Conclusion

In this work, we have analyzed the thermal and vibration effect on the space re-entry vehicle returning to the Earth's temperature. These materials withstand the high temperature produced on the space re-entry vehicle due to aero thermodynamic heating caused by shock waves. The silica aerogel is a lightweight material that can

DOI: http://dx.doi.org/10.5772/intechopen.107841

withstand very high temperatures and has reduced wear and tear effects on the body of the space re-entry vehicle. Since silica aerogel material is not reacted with any other substance, by keeping silica aerogel as outer layer-1, PICA as layer-2, TUFROC as layer-3, and UHTC as an innermost layer-4, these sandwich-like layered structures will exhibit excellent heating ablating, vibration absorbing properties, and good durability so that it can be utilized as heat shielding materials for long time processes as that can reduce the cost of material used for the heat shield. Using an aerospike in a re-entry vehicle will reduce the strength of the shockwave formation. Thereby, there will be a better reduction in the aerothermodynamics heating. So, employment of aerospike in the re-entry vehicle will effectively reduce the cost due to structural damages and therefore, it will be an innovative and effective design concept for future developments.

Author details

Pradeep Kumar Sulur Loganathan
Department of Aeronautical Engineering, KIT-Kalaignarkarunanidhi Institute of Technology, Tamil Nadu, India

*Address all correspondence to: pradeepzero1991@gmail.com

References

[1] Chang FY, Weng HC. Hypersonic thermal flow past a spherically blunted tangent-ogive nose cone. Journal of Chinese Society of Mechanical Engineering. 2022;**43**(1):1-10

[2] Wu J, Zhang Z, Hou A, Xue X, Cao X. Thermal aeroelastic characteristics of inflatable reentry vehicle experiment (IRVE) in hypersonic flow. International Journal of Aerospace Engineering. 2021; **2021**:1-17

[3] Moreira FC, Wolf WR, Azevedo JLF. Thermal analysis of hypersonic flows of carbon dioxide and air in thermodynamic non-equilibrium. International Journal of Heat and Mass Transfer. 2021;**165**:1-19

[4] Di Fiore F, Maggiore P, Mainini L. Multifidelity domain-aware learning for the design of re-entry vehicles. Structural and Multidisciplinary Optimization. 2021;**64**(5):3017-3035. DOI: 10.1007/s00158-021-03037-4

[5] Di Caprio F et al. Damage tolerance evaluation of a C/C-SiC composite body flap of a re-entry vehicle. Composite Structures. 2021;**274**:114341

[6] Farah E, Teschner T-R. Aerodynamic performance investigation through different chemistry modelling approaches for space re-entry vehicles using the DSMC method. In: UKACM 2022 2022 Annu. Conf. UK Assoc. Comput. Mech. Nottingham, UK. 2022

[7] Delfini A et al. Thermal analysis of advanced plate structures based on ceramic coating on carbon/carbon substrates for aerospace Re-Entry Re-Useable systems. Acta Astronautics. 2020;**183**:153-161

[8] Mallick A, Kapadia B, Arnold A. A brief discussion about reentry vehicles. International Journal of Latest Engineering Management Research. 2017;**02**(02):50-63

[9] Ma H, Zheng X, Luo X, Yi Y, Yang F. Simulation and analysis of mechanical properties of silica aerogels: From rationalization to prediction. Materials (Basel). 2018;**11**(2):1-12. DOI: 10.3390/ma11020214

[10] Balakrishna B, Venkateswarlu S, Reddy PR. Flow analysis of an atmosphere re-entry vehicle. International Journal of Engineering Research and Development. 2012;**3**(4):2278-2267

[11] Wuchina E, Opila E, Opeka M, Fahrenholtz W, Talmy I. UHTCs: Ultra-high temperature ceramic materials for extreme environment applications. Electrochemical Society Interface. 2007;**16**(4):30-36. DOI: 10.1149/2.f04074if

[12] Krishna S, Student PG. Coupled field analysis of nose cone of a re-entry vehicle. International Journal of Research & Computational Technology. 2015;**7**(5):14-24

[13] Bheekhun N, Abu Talib AR, Hassan MR. Aerogels in aerospace: An overview. Advanced Materials in Science and Engineering. 2013;**2013**:1-19

[14] Prasanna Kumar TJ, Dharma Teja R, Rajesh R, Karthi AR. Transient thermal analysis on re-entry vehicle nose cone with tps materials. International Journal of Aerospace in Mechanical Engineering. 2016;**3**(6):6-15

[15] Macias C et al. Synthesis of porous and mechanically compliant carbon aerogels using conductive and structural additives. Gels. 2016;**2**(1):1-16. DOI: 10.3390/gels2010004

[16] Carandente V, Savino R, Iacovazzo M, Boffa C. Aerothermal analysis of a sample-return re-entry capsule. Fluid Dynamic Material Process. 2013;**9**(4):461-484. DOI: 10.3970/fdmp.2013.009.461

[17] Raju M. CFD analysis of mars phoenix capsules at Mach number 10. Journal of Aeronautical Aerospace Engineering. 2015;**04**(01):4-7. DOI: 10.4172/2168-9792.1000141

[18] Shaid A, Furgusson M, Wang L. Thermophysiological comfort analysis of aerogel nanoparticle incorporated fabric for fire fighter's protective clothing. Chemical Materials Engineering. 2014; **2**(2):37-43

[19] Thapliyal PC, Singh K. Aerogels as promising thermal insulating materials: An overview. Journal of Materials. 2014;**2014**:1-10. DOI: 10.1155/2014/127049

[20] Hoseini A, McCague C, Andisheh-Tadbir M, Bahrami M. Aerogel blankets: From mathematical modeling to material characterization and experimental analysis. International Journal of Heat and Mass Transfer. 2016;**93**:1124-1131. DOI: 10.1016/j.ijheatmasstransfer.2015.11.030

[21] Ibrahim M et al., Aerogel-based coating for energy-efficient building envelopes To cite this version: HAL Id : hal-01112594. 2015

[22] Jelle BP, Baetens R, Gustavsen A. Aerogel insulation for building applications. Sol-Gel Handbook. 2015;**3–3**:1385-1412. DOI: 10.1002/9783527670819.ch45

[23] Patel RP, Purohit NS, Suthar AM. An overview of silica aerogels. International Journal of ChemTech Research. 2009; **1**(4):1052-1057

[24] Cohen E, Glicksman L. Thermal properties of silica aerogel formula. Journal of Heat Transfer. 2015;**137**(8):111

[25] Zhao Z, Wang X, Qiu J, Lin J, Xu D. Three-dimensional graphene-based hydrogel. Aerogel Materials. 2014;**36**: 137-151

[26] Chakraborty S, Pisal AA, Kothari VK, Venkateswara Rao A. Synthesis and characterization of fibre reinforced silica aerogel blankets for thermal protection. Advanced Materials in Science and Engineering. 2016; **2016**:1-9

[27] Tsioulou O, Erpelding J, Lampropoulos A. Development of novel low thermal conductivity concrete using aerogel powder. 2016

[28] Venkatapathy E et al. Sustaining mature thermal protection systems crucial for future in-situ planetary missions. Bulletin AAS. 2021;**53**(4):7. DOI: 10.3847/25c2cfeb.8dd247ac

[29] Ford K, Meurisse MJ, Thornton J. Sensitivity Analysis of PICA and PICA-N Using PATO and DAKOTA. 2021

[30] Arenas JP, Crocker MJ. Recent trends in porous sound-absorbing materials. Sound & Vibration. 2010; **44**(7):12-18

[31] Lynam A, Romero AR, Xu F, Wellman RW, Hussain T. Thermal spraying of ultra-high temperature ceramics: A review on processing routes and performance. Journal of Thermal Spray Technology. 2022;**31**(4):745-779. DOI: 10.1007/s11666-022-01381-5

[32] Lin MF. Thermal properties of carbon toroids. Journal of the Physical Society of Japan. 1999;**68**(11):3585-3591. DOI: 10.1143/JPSJ.68.3585